

Research Paper

# Projected Climate Indices Impact on the Hydrology Process in the Bago River Basin, Myanmar

S. W. Thin <sup>1</sup>, K. Ohgushi <sup>2</sup>

## ARTICLE INFORMATION

### Article history:

Received: 5 December, 2022

Received in revised form: 10 February, 2023

Accepted: 15 February, 2023

Publish on: 20 February, 2023

### Keywords:

Bago River Basin  
Climate Indices  
Bias Correction  
Correlation Analysis  
Trend Analysis  
Hydrological components



This work is licensed under a Creative Commons Attribution-NonCommercial 4.0 International License.

## ABSTRACT

Despite the impact of temperature and precipitation patterns on river flows is an emerging issue in hydrology, few studies have been concentrated on the correlation between the hydrological components and climate indices. This study mainly focuses on the projected extreme climate indices and the effects of climate change projections on the hydrological process in the Bago River Basin, Myanmar. It has been noted that the mean monthly maximum temperature values are expected to rise throughout the entire basin under the RCP 4.5 scenario. On the other hand, the annual total precipitation index is anticipated to increase. The findings imply that the groundwater and surface flow will eventually expand as a result of the effects of extreme precipitation indices. Subsequently, there will be a decrease in the lateral flow. Furthermore, it is observed that the effect of temperature indices will cause a significant impact on evapotranspiration. This paper highlights that the crucial part of the extreme climate indices that influence the regional hydrological processes of the Bago River Basin in the upcoming decades.

## 1. Introduction

Floods and drought are undeniable subsequences of climate change effect. Likewise, it influences the water balance of the hydrological cycle. Therefore, it is essential to comprehend how climate change projections will affect the hydrological process. In order to generate the climate projections, the General Circulation Models, also known as global climate models (GCMs) are vital role to predict under different emission scenarios (Mishra et al., 2020; Aguayo et al., 2021). The GCMs are mathematical models and contain many different earth systems, including the atmosphere, oceans, land surface,

etc. They can assist to provide the prospective outcomes for study on climate change and variability. They are typically available with spatial resolutions of 2° and 4°, and are subject to uncertainty originating from multiple sources (Singh et al., 2019). Their accuracies decline at finer spatial scales, and some of their observations are very inaccurate when applied to a small scale (Singh et al., 2016; Chen et al., 2012). Regarding to the regional and practical applications, (Raju et al., 2020) highlighted that GCMs have some uncertainties to predict for the future projections of water resources. Additionally, when applying GCMs to function together with hydrological implications on climate change, the simulated outputs are

<sup>1</sup> Doctoral Student, Department of Civil Engineering and Architecture, Faculty of Science and Engineering, Saga University, Saga, JAPAN, 20695907@edu.cc.saga-u.ac.jp

<sup>2</sup> Professor, Department of Civil Engineering and Architecture, Faculty of Science and Engineering, Saga University, Saga, JAPAN, ohgushik@cc.saga-u.ac.jp

not well agreed with the observed ones (Kundzewicz et al., 2022).

Moreover, climate indices are the parameters to track changes in the frequency of extreme weather events. The Expert Team on Climate Change Detection Indices (ETCCDI) of the Commission for Climatology, the World Climate Research Program, and the Technical Commission for Oceanography and Marine Meteorology (CCI /WCRP/JCOMM) created the total 27 indices based on the consideration of daily temperature values or daily precipitation quantities (Zhang et al., 2005; Pesce et al., 2022). In the "climate literature", ETCCDI indices are frequently employed to evaluate statistics of temperature and precipitation extremes, and it can be used to examine a range of extreme phenomena, including heavy rain, floods, droughts, heat waves, etc. In particular, it may be essential for identifying future changes by applying projections from climate models to investigate the climatic impact (Sardella et al., 2020).

Due to the effects of climate change, the Bago River Basin has recently experienced numerous floods and droughts (Hlaing et al., 2008). The water supplies from this river basin are essential to the regular farming and fishing operations of the local residents. Approximately, a third of the local residents utilize the agricultural area of over 890 km<sup>2</sup> annually. Typically, in summer and rainy seasons, water shortage and flooding are common problems during cultivation and harvesting (Htut et al., 2015).

In order to overcome this frequent issue, it is still necessary to examine the climatic data in all aspects so that it can predict the hydrological process in more detail. Many previous studies (Htut et al., 2014; Shrestha et al., 2016; Shrestha et al., 2014 and 2017; Myo et al., 2020) have been used to assess the impact of climate change using precipitation and temperature variables under different scenarios and demonstrated streamflow changes for past and future periods in the Bago River Basin, Myanmar. Furthermore, there have been few studies to investigate the long-term changes in climate patterns and extreme climate parameters utilizing ETCCDI extreme climatic indices over time in Myanmar (Kyu et al., 2016; Sein et al., 2018; and Kyaw et al., 2022). However, it is critical to consider more extreme climate indices that are strongly correlated with climate variables and water balance components in the hydrological process in a specific region. Therefore, this study examined the probable future extreme climate trends and variability of water balance components using each extreme climatic indicator in the Bago River Basin, Myanmar.

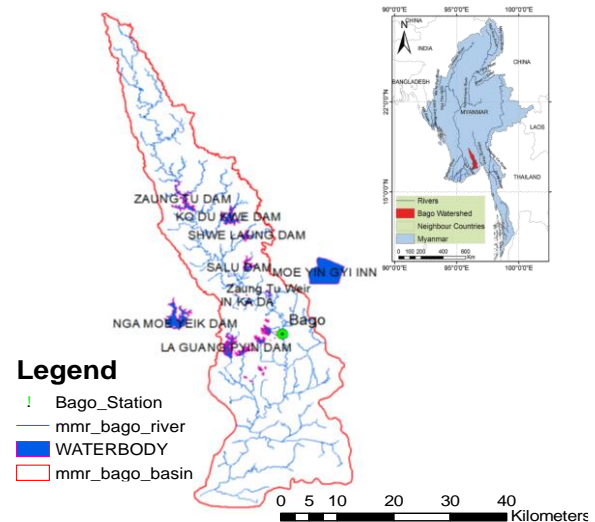


Fig. 1. Location of the Bago River Basin (Shelly et al., 2014).

## 2. Study area and datasets

### 2.1 Study Area

The Bago River Basin is one of the most important and useful river basins in lower Myanmar for hydropower generation, irrigation, fisheries and navigation purposes. According to the government's census, the total population of the Bago River Basin in 2010 was 5.327 million, with a population density of 1,091 people/km<sup>2</sup>. The local populations are mainly composed of 40% for farmers and 30% for fishermen. With a total area of 4,883.1 km<sup>2</sup>, this river basin covers 91% of the Bago district (Shelly et al., 2014). The basin area is located between latitudes 16° 42' 00" and 18° 30' 00" N and longitudes 95° 42' 00" and 96° 00' 00" E (Shelly et al., 2020). In this basin, a hydropower dam for electricity and irrigation, Zaung Tu Dam, were constructed in 1996. For the purpose of flood control during the rainy season and the irrigation water use for summer paddy cultivation, three earthen dams namely Kodukwe, Salu, Shwelaung were constructed and opened in May, 2012. The location map of the Bago River Basin is shown in Figure 1.

The effects of climate change became apparent in this basin at the beginning of the 21<sup>st</sup> century. The main impacts of climate change in this basin are increased surface runoff, land cover change, deforestation, and soil erosion (Kawasaki et al., 2017). As a result, the local people are becoming increasingly affected to food security, water scarcity, and poverty as well. Additionally, it is expected that variations in temperature and precipitation will have significant effects on the water resources. Therefore, this study examines the projections of the impact of extreme climate indicators on the hydrological cycle in the Bago River Basin, Myanmar.

## 2.2 Hydro-climatic data

### 2.2.1 Observed Data

The Bago River Basin has a tropical monsoon climate, warm temperatures and distinct wet and dry seasons. According to weather databases, in 1997, the average annual precipitation occurred the highest amount of 3,143 mm during the past 30 years (1975-2005) (Shelly et al., 2020; Kawasaki et al., 2017). This river basin experienced an average annual rainfall of 2,980 mm over the baseline period (1981–2000), with 130 rainy days on average per year as well. In order to conduct the research analysis, temperature and precipitation data at the Bago station for the period during 1981 to 2000 were obtained from the Department of Meteorology and Hydrology in Myanmar. The daily discharge data during 1981 to 2000 and 2010 to 2014 was provided by this department (Department of Meteorology and Hydrology, Myanmar). The monthly distribution of precipitation is directly related to the southwest monsoon. In recent decades, there has been a gradual increase in the frequency and magnitude of extreme circumstance. When extreme climate change simultaneously occurs, both droughts and floods drastically alter livelihoods.

### 2.2.2 GCMs Data

The Fifth IPCC Assessment Report (AR5) launched CMIP5 in 2013 (Allen et al., 2013). This is the main framework for coordinated climate modeling experiments. The CMIP5 experimental rules provides four emissions scenarios based on the Representative Concentration Pathways (RCPs) identified by the amount of net radiative forcing on the global climate system at the end of the 21<sup>st</sup> century (IPCC, 2001). There have been conducted some studies in recent years to verify the selection criteria for GCMs. According to the selection of GCMs in the Bago River Basin (Htut et al., 2015; Zwiers et al., 2009), the five distinct GCM models under scenario RCP 4.5 were taken into consideration for the analysis of climate projections in this research (Table 1).

### 2.3 Climate Indices

There is a growing need for science-based information about weather and extreme climates. The Joint Expert Team on Climate Change Detection and Indicators (ETCCDI) has delineated a core set of extreme descriptive indicators to provide a unified perspective on observed weather changes and climate extremes (Brown et al., 2010; Zhang et al., 2011; Afzal et al., 2015; Pat et al., 2018; Aryal et al., 2020; Chapagain et al., 2021; Charles et al., 2022). In this research, six climate indices and five climate indices based on precipitation and

**Table 1.** A list of the climate models used in this research, in addition to a summary of each model's resolution, model description and each climate change scenario (Coupled Model Intercomparison Project Phase 5 (CMIP5)).

Models	Model Description and Research Center	Resolution (Degree)	Projection
BCC-CSM1.1	Climate System Model Version 1, Beijing Climate Center	128×64	RCP 4.5
CCSM4	The community Climate System Model Version 4, National Center for Atmospheric Research USA	288×192	RCP 4.5
CNRM-CM5	Centre National de Recherches Météorologiques Climate Model version 5, CNRM/Center Européen de Recherche et Formation Avancée en Calcul Scientifique, France	256×128	RCP 4.5
GISS-E2R	Goddard Institute for Space Studies Model E version 2 with Russell Ocean Model, GISS, National Aeronautics and Space Administration, USA	144×90	RCP 4.5
MRI-CGCM3	Meteorological Research Institute Coupled General Circulation Model Version 3, MRI, Japan	320×160	RCP 4.5

maximum and minimum temperatures at specified station indicated by ETCCDI are calculated. The minimum and maximum temperature values and intensity indices, such as SU, TNn, TNx, TXn and TXx were examined. Whereas SDII, R95PTOT, R99PTOT, CWD and CDD are considered for assessing variations in climatic extremes, PRCPTOT is an index used to represent the mean state of the climate. The extreme daily precipitation indices, R95PTOT and R99PTOT, are determined by using a limit that correlates to the precipitation values of the 95% and 99% percentiles. The process used to calculate each climate indices and units are shown in Table 2 (a) and Table 2 (b).

### 2.4 Method of correlation

In order to assess the accuracy, the two types of data objects are compared attribute by attribute. The correlation score is obtained by adding the squares of the

**Table 2 (a).** Description of climate indices for the variable of precipitation

Variable	Indices	Description	Unit
Precipitation (Pr)	PRCPTOT	Annual Total Precipitation in Wet Days (mm)	mm
	SDII	Simple Precipitation Intensity Index	mm/day
	R95PTOT	Annual Total Precipitation when daily precipitation is greater than the 95th percentile	mm
	R99PTOT	Annual Total Precipitation when daily precipitation is greater than the 99th percentile	mm
	CDD	Maximum length of dry spell (number of consecutive dry days)	day
	CWD	Maximum length of wet spell (number of consecutive wet days)	day

**Table 2 (b).** Description of climate indices for the variable of temperature

Variable	Indices	Description	Unit
Temperature (T)	SU	Number of summer days (daily maximum temperature >25°C)	day
	TNx	Annual maximum value of daily minimum temperature	°C
	TXx	Annual maximum value of daily maximum temperature	°C
	TXn	Annual minimum value of daily maximum temperature	°C
	TNn	Annual minimum value of daily minimum temperature	°C

magnitude differences between the two attributes. One of the most popular correlation methods, Pearson’s correlation, produces a value that can vary from -1 to +1. A high score (near +1) denotes the great degree of similarity between both data (Christensen et al., 2008; Teutschbein et al., 2010; Taylor et al., 2012). A Pearson score close to 0 would be observed for any uncorrelated data. This score close to 1 would indicate that the two data are inversely correlated (i.e., one is decreasing when the other is increasing). In order to calculate the Pearson’s correlation coefficient was shown in Eq. (1) (Lenderink et al., 2007).

$$r = \frac{n(\sum_{i=1}^n xy) - (\sum_{i=1}^m x)(\sum_{i=1}^n y)}{\sqrt{[n\sum_{i=1}^m x^2 - (\sum_{i=1}^m x^2)][n\sum_{i=1}^n y^2 - (\sum_{i=1}^n y^2)]}} \quad (1)$$

where r is the Pearson correlation coefficient, x is the value in the first set of the data, y is the value in the

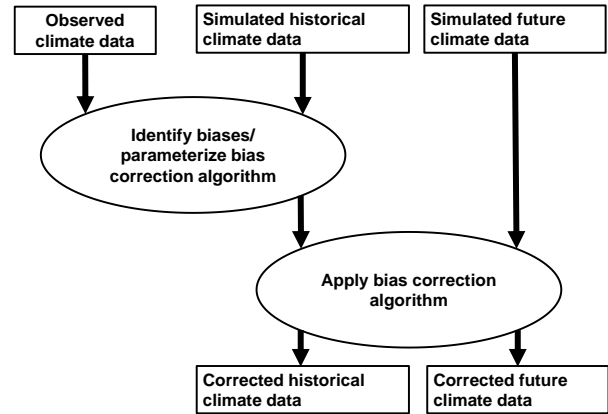


**Fig. 2.** Bias correction framework in the CMhyd (Rathjens et al., 2016; Dietzsch et al., 2017)

second set of the data, and n is the total number of values.

**2.5 Bias Correction Procedures**

Correction techniques are required because climate models frequently generate distorted representations of observed time series (Lenderink et al., 2007; Deser et al., 2012; Ahmadalipour et al., 2018). The bias correction methods employ a transformation technique to modify the GCM output. The main concept of corresponding both controls and scenario GCM runs is to identify the potential biases between the observed and simulated climatic variables (Song et al., 2020; Song et al., 2022; Yang et al., 2023). In this research, the CMhyd (Climate model data for hydrologic modeling) (Rathjens et al., 2016) was examined to simulate the climatic data collected from GCMs. The CMhyd conducts the data preparation before bias correction. It is performed to ensure that the grid cells of the climate model are situated where they are supposed to be significantly closer regarding to the gauges. Moreover, the performance is evaluated by contrasting the observed data and the modelled one. This is followed by combining the observed and modelled data periods (Yeboah et al., 2022; Olsson et al., 2016). In this study, two bias correction techniques such as linear-scaling and delta-change approach method for variations in temperature and precipitation were examined. The bias corrections have been performed using the CMhyd tool extensively in various applications. Figure 2 (Dietzsch et al., 2017) illustrates the overall bias correction procedure used in this paper.

**2.5.1 Linear-scaling approach**

The linear-scaling strategy is operational using the monthly correction values based on the variations between the observed and simulated values. The GCMs from climate models are still needed to be corrected to

produce simulations that exactly match the observations (Christensen et al., 2008; Li et al., 2017; Jose et al., 2022; Oruc et al., 2022). A factor based on the proportion of long-term monthly mean observed and control run data is used to adjust precipitation. Based on the difference between the long-term monthly mean observed and control run data, the temperature is corrected using an additive term that presented from Eq. 2 to Eq. 5.

$$P_{contr}^*(d) = P_{contr}(d) \cdot [\mu_m(P_{obs}(d)) / \mu_m(P_{contr}(d))] \quad (2)$$

$$P_{scen}^*(d) = P_{scen}(d) \cdot [\mu_m(P_{obs}(d)) / \mu_m(P_{contr}(d))] \quad (3)$$

$$T_{contr}^*(d) = T_{contr}(d) + \mu_m(T_{obs}(d)) - \mu_m(T_{contr}(d)) \quad (4)$$

$$T_{scen}^*(d) = T_{scen}(d) + \mu_m(T_{obs}(d)) - \mu_m(T_{contr}(d)) \quad (5)$$

where  $P_{contr}^*(d)$  and  $P_{scen}^*(d)$  are corrected precipitation data during the control period (past period) and scenario period (future period), respectively,  $P_{contr}(d)$  and  $P_{obs}(d)$  are raw and observed precipitation data during the control period (past period), respectively,  $\mu_m$  is a monthly mean value,  $T_{contr}^*(d)$  and  $T_{scen}^*(d)$  are corrected temperature data during the control period (past period) and scenario period (future period), respectively,  $T_{contr}(d)$  and  $T_{obs}(d)$  are raw and observed temperature data during the control period (past period), respectively.

### 2.5.2 Delta-change method

The delta-change method simulates future changes for a perturbation of observable data rather than directly employing the simulations of future (Lenderinl et al., 2007; Jose et al., 2022; Oruc et al., 2022; Linling et al., 2023). In the future scenario, the observational time series is superimposed with the simulated data comparing the control and the runs. Generally, the bias correction method is calculated from Eq. 6 to Eq. 9.

$$P_{Contr}^*(d) = P_{contr}(d) \quad (6)$$

$$P_{scen}^*(d) = P_{scen}(d) \cdot [\mu_m(P_{scen}(d)) / \mu_m(P_{contr}(d))] \quad (7)$$

$$T_{Contr}^*(d) = T_{contr}(d) \quad (8)$$

$$T_{scen}^*(d) = T_{scen}(d) + \mu_m(T_{scen}(d)) - \mu_m(T_{contr}(d)) \quad (9)$$

### 2.6 Trend analysis

The trend analysis is required to identify and quantify the extent of trends in a dataset. Dataset trends can either be step trends, where the changes in statistics may

occur at a certain duration, or monotonic trends, where a variable constantly increases or decreases over time (Nie et al., 2019; Hirsch et al., 1982).

The trend in the extreme precipitation and temperature indices is examined using the non-parametric Mann-Kendall (MK) trend test (Kendall et al., 1975; Benestad et al., 2004). This method is frequently applied to detect patterns in the time series of hydro-meteorological data defined by;

$$S = \sum_{i=1}^{n-1} \sum_{j=i+1}^n \text{sign}(x_j - x_i) \quad (10)$$

$$\text{sign}(x_j - x_i) = \begin{cases} +1, & \text{if } (x_j - x_i) > 0 \\ 0, & \text{if } (x_j - x_i) = 0 \\ -1, & \text{if } (x_j - x_i) < 0 \end{cases} \quad (11)$$

where, in the time series of size  $n$ ,  $x_j$  and  $x_i$ , respectively, represent the  $j$ th and  $i$ th terms. The  $S$  is obtained in Eq. 10 as the number of positive differences minus the number of negative differences. Therefore, a positive  $S$  indicates that there is an increasing tendency in the data because the most existing data is larger than the previous data, whereas a negative  $S$  indicates the opposite (Eq. 11). For  $n > 10$ , the average  $E$ , and the variance (Var) of  $S$  are describe as shown in Eq. 12 and Eq. 13.

$$E(S) = 0 \quad (12)$$

Whereas Kendall (Kendall et al., 1975) has already demonstrated that  $S$  is asymptomatic and regularly distributed for time series with  $n > 10$ , where the mean is 0.

$$\text{Var}(S) = \frac{1}{18} \left[ n(n-1)(2n+5) - \sum_{i=1}^m t_i(t_i-1)(2t_i+5) \right] \quad (13)$$

where  $t_i$  is the quantity of data in the  $i$ th tied group, and where  $m$  is the total number of tied groups in the time series. The Eq. 14 is used to obtain the normal  $Z$  test statistic by

$$Z = \frac{S \pm 1}{\text{Var}(S)^{1/2}} \quad (14)$$

The variables used in Eq. 14 are  $S-1$  if  $S > 0$ ,  $S+1$  if  $S < 0$ , and  $Z$  is 0 if  $S = 0$  (Duhan et al., 2013; Yacoub et al., 2019; Feliz et al., 2021). The rising trend is indicated by a positive  $Z$  value. In different circumstances, it suggests a decreasing tendency. The null hypothesis is rejected in order to test for either an increasing or a decreasing monotonic trend at the  $p$  significant level. The magnitude of the trend's slope can also be estimated non-

parametrically. Since the significance level ( $\alpha$ ) is higher than the calculated p-value ( $0.05 > 0.0001$ ), this denotes a trend that is significantly increasing at a 5% level of significance.

### 3. Setup of simulations

The GCMs are used to evaluate the impacts of climatic variability and change. The output of GCMs has a coarse spatial resolution, which makes it difficult to use them (Benestad et al., 2004). Additionally, as a consequence of the GCMs' description of spatial resolution, bias correction is necessary to apply for many hydrological applications (Rauscher et al., 2013). The statistical transformation is the foundation of bias correction methods, which focus on making the distribution modeled data more accurately reflect the observed climatology. The bias correction techniques for the historical temperature and precipitation of five GCMs for hydrological application were initially performed.

Furthermore, it was assessed whether the climatic indices that used GCMs performed over the past period (1981-2000). The evaluation of spatial correlations is determined in accordance with the standards (Gassman et al., 2007), which state that correlations of 0.4 or less imply very poor model performance, correlations between 0.4 and 0.6 reflect the fact of acceptable capability, correlations between 0.6 and 0.7 clearly show satisfactory performance, correlations between 0.7 and 0.85 appear to suggest great skill, and correlations of 0.85 or more demonstrate extremely good model advancement. According to this standard, the outcomes are arranged for the projected changes that the distribution of each future period (2040-2059 and 2060-2079) under the RCP 4.5 and the past period (1981-2000). In order to simulate the hydrological process, a calibrated Soil Water Assessment Tool (SWAT), hydrological model was applied as input to five statistically bias-corrected GCMs under the historical and RCP 4.5 scenario. Figure 3 shows the schematic plan of the projected impact of climate on the hydrological processes in the Bago River Basin, Myanmar.

The hydrological river basin model known as SWAT can be used to generate a wider range of watershed scenarios (Gassman et al., 2007). The physical or conceptual models, alongside the corresponding variables, are integrated into the model to simulate a number of environmental factors in a watershed: (1) climatic simulation, including meteorological conditions, air, soil, and water temperatures, solar radiation, wind speed, rainfall, snowmelt, water droplets, relative humidity; (2) simulation of hydrological processes, such as estimation of discharge using the widely used SCS

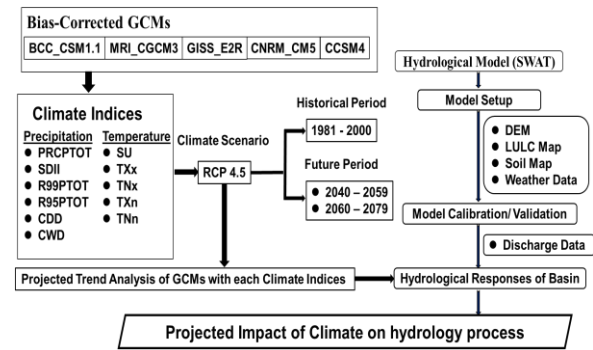


Fig. 3. Schematic diagram of simulation procedures.

(Soil Conservation Service) method, evapotranspiration by using Penman-Monteith method, actual evapotranspiration, and water movement in the unsaturated and saturated zone; (3) simulation of sediment materials for erosion and discharge; (4) simulation of crop growth and cultivation methods and practices; and (5) simulation of flowing water and pollution in watercourses (Gassman et al., 2007; Silva et al., 2015). The river basin is divided into a variety of sub-basins and then into a number of HRUs (Hydrological Response Units) in the SWAT model. The hydrological water balance is the first and necessary component for each model in SWAT. The water balance accelerates every process that actually occurs in the river basin. The water balance is calculated in Eq. 15.

$$SW_t = SW_0 + \sum_{i=1}^n (R_{day} - Q_{surf} - ET_i - Q_{seep} - Q_{gw}) \quad (15)$$

where  $SW_t$  is the final soil water content (mm water),  $SW_0$  is the beginning soil water content (mm water), and  $R_{surf}$  is the surface runoff (mm water) on a given day;  $P_{day}$  is for precipitation on day  $i$  (mm of water), and  $ET_i$  stands for the amount of evapotranspiration on day  $i$ .  $Q_{seep}$  is the quantity of water entering the unsaturated zone of soil on day  $i$  (mm), and  $Q_{gw}$  is for return flow on day  $i$  (mm of water).

## 4. Results and discussion

### 4.1 Evaluation of GCMs

The bias correction strategy using the linear scaling and delta-change approach were explored in contrast to the original GCMs output data. Figure 4 (a) shows the Taylor diagram for the average monthly precipitation using the observed data and two bias-corrected GCMs (linear scaling and delta-change approach methods) as the reference value for the past period (1981–2000). The Pearson's coefficient of precipitation data for GCMs (CNRM-CM5, BCC-CSM1.1, MRI-CGCM3, GISS-E2R, and CCSM4) using the linear scaling and delta-change-

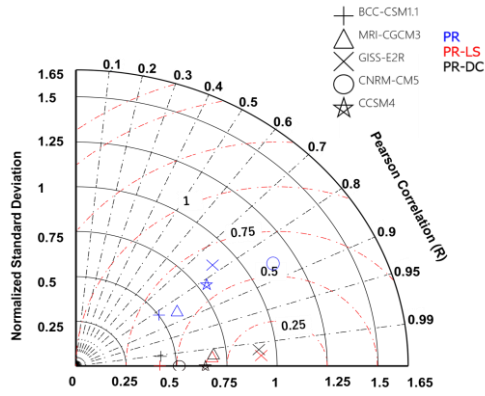


**Fig. 4(a).** Taylor diagram indicating the performance Precipitation (PR) of five GCMs using Linear scaling and Delta Change bias corrected data and original data.

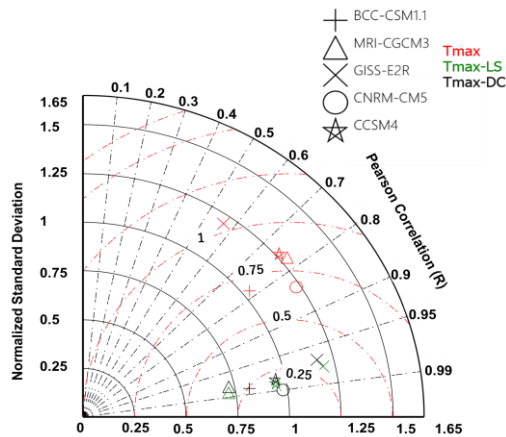


**Fig. 4(b).** Taylor diagram indicating the performance maximum Temperature (Tmax) of five GCMs using Linear scaling and Delta Change bias corrected data and original data.

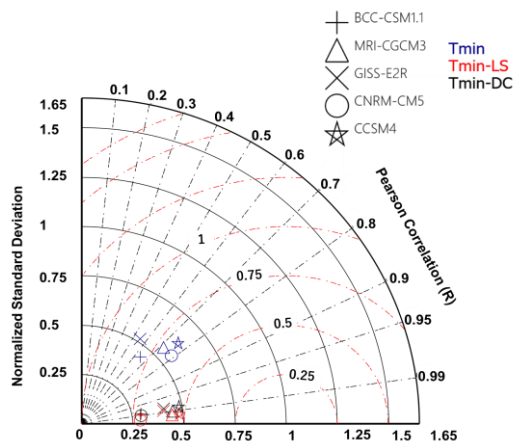


**Fig. 4(c).** Taylor diagram indicating the performance minimum Temperature (Tmin) of five GCMs using Linear scaling and Delta Change bias corrected data and original data.

approach methods over the past period is 0.85, 0.75, 0.7, 0.65, 0.65, and 0.85, 0.7, 0.75, 0.7, 0.7, respectively. Similar to this, the Taylor diagrams are shown in Figure 4 (b) and Figure 4 (c) for the mean monthly maximum

temperature (Tmax) and mean monthly minimum temperature (Tmin), respectively. The Pearson's coefficient of maximum and minimum temperatures for all GCMs is indeed around 0.85 after utilizing two bias correction techniques.

The correlation coefficients demonstrate that the delta-change method of bias reduction does not deviate significantly from linear scaling method. While bias corrections are added, the mean monthly maximum and minimum temperatures and precipitation have substantial correlation coefficients that are approaching to unity. These findings express that the bias correction techniques can be utilized effectively for temperature variable as well as precipitation variable for the Bago River Basin, Myanmar.

#### 4.2 Trend Analysis of Extreme Climate Indices

##### 4.2.1 Precipitation

The trend analysis was conducted by estimating the annual data from the observed and GCMs using the precipitation indices. The trend test, a nonparametric MK trend, was performed based on extreme index values to detect temporal trends and significant levels over the past period (1981 to 2000). This analysis ultimately assists to identify the effects of climate change on extreme climate index trends. Table 3, Table 4 and Table 5 show the correlation matrices for each climate index using the GCM output for past period (1981-2000) and future periods (2040-2059 and 2060-2079). The observed annual total precipitation climate index (RPCPTOT) corresponds to a significantly correlated climate index using GCM results over the past period. The precipitation intensity (SDII) over the past and future periods shows the strongest correlation during the extreme rainfall circumstances.

Figure 5 to Figure 10 display the findings of the annual trend analysis of all precipitation indices at the Bago station during the past and future periods. There were observed the increasing and decreasing trends for extreme precipitation climatic indices. The PRCPTOT index shows a most positive slope, which indicates an increasing trend in future periods (Figure 5). According to the results of the precipitation intensity index trend, there has been a trend toward a slight reduction in the future (Figure 6). It implies that the future periods will experience an increase in the amount of precipitation. Moreover, the trends in the contribution of the days with daily precipitation above the 99<sup>th</sup> percentile (R99PTOT) show an upward tendency in extremely wet days over the past period. The 99<sup>th</sup> percentile trends for the future periods 2040-2059 and 2060-2079 increased in comparison to the 95<sup>th</sup> percentile trend (Figure 7 and

Figure 8). In both periods, consecutive wet days (CWD) are computed with decreasing trends (Figure 9). Additionally, an increasing tendency in the CDD index for upcoming periods has been observed (Figure 10).

**Table 3.** Correlation matrix of 11 climate indices using five GCMs during the past period (1981-2000).

Indices (BCC-CSM1.1)	PRCPTOT	SDII	R95PTOT	R99PTOT	CWD	CDD	SU	TNx	TXx	TXn	TNn
PRCPTOT	1	0.55	0.40	0.06	0.21	-0.40	-0.25	-0.04	-0.02	-0.10	0.26
SDII	0.55	1	0.40	0.29	0.28	-0.06	0.08	0.08	0.46	0.05	0.45
R95PTOT	0.40	0.40	1	0.30	0.31	-0.33	0.28	0.02	0.30	0.14	0.23
R99PTOT	0.06	0.29	0.30	1	0.17	-0.13	0.13	0.43	0.37	-0.21	-0.05
CWD	0.21	0.28	0.31	0.17	1	0.22	0.05	-0.10	0.02	0.10	-0.24
CDD	-0.40	-0.06	-0.33	-0.13	0.22	1	0.04	0.33	0.04	0.07	-0.35
SU	-0.25	0.08	0.28	0.13	0.05	0.04	1	0.13	0.10	0.05	0.40
TNx	-0.04	0.08	0.02	0.43	-0.10	0.33	0.13	1	0.20	0.02	-0.18
TXx	-0.02	0.46	0.30	0.37	0.02	0.04	0.10	0.20	1	0.14	0.22
TXn	-0.10	0.05	0.14	-0.21	0.10	0.07	0.05	0.02	0.14	1	0.05
TNn	0.26	0.45	0.23	-0.05	-0.24	-0.35	0.40	-0.18	0.22	0.05	1

Indices (MRI-CGCM3)	PRCPTOT	SDII	R95PTOT	R99PTOT	CWD	CDD	SU	TNx	TXx	TXn	TNn
PRCPTOT	1	0.28	0.29	0.12	-0.49	0.01	0.09	0.21	0.12	0.21	-0.06
SDII	0.28	1	0.04	0.30	0.09	0.24	0.07	-0.12	0.27	0.16	-0.18
R95PTOT	0.29	0.04	1	0.14	0.07	-0.51	-0.05	0.19	-0.11	-0.14	0.42
R99PTOT	0.12	0.30	0.14	1	-0.04	-0.08	0.20	-0.15	0.01	0.25	-0.09
CWD	-0.49	0.09	0.07	-0.04	1	0.23	0.12	-0.15	0.04	-0.04	0.22
CDD	0.01	0.24	-0.51	-0.08	0.23	1	0.20	-0.24	0.12	0.23	-0.21
SU	0.09	0.07	-0.05	0.20	0.12	0.20	1	0.04	-0.15	0.79	0.49
TNx	0.21	-0.12	0.19	-0.15	-0.15	-0.24	0.04	1	-0.15	-0.05	0.29
TXx	0.12	0.27	-0.11	0.01	0.04	0.12	-0.15	-0.15	1	-0.38	-0.47
TXn	0.21	0.16	-0.14	0.25	-0.04	0.23	0.79	-0.05	-0.38	1	0.33
TNn	-0.06	-0.18	0.42	-0.09	0.22	-0.21	0.49	0.29	-0.47	0.33	1

Indices (GISS-E2R)	PRCPTOT	SDII	R95PTOT	R99PTOT	CWD	CDD	SU	TNx	TXx	TXn	TNn
PRCPTOT	1	0.29	0.34	0.36	-0.07	0.09	-0.12	0.07	0.04	0.28	0.04
SDII	0.29	1	0.45	0.68	0.33	0.16	-0.16	0.00	0.23	0.03	0.17
R95PTOT	0.34	0.45	1	0.33	0.30	0.44	-0.21	0.23	0.00	-0.03	-0.01
R99PTOT	0.36	0.68	0.33	1	0.17	-0.15	-0.35	0.08	0.05	0.13	0.10
CWD	-0.07	0.33	0.30	0.17	1	0.44	0.10	-0.11	0.00	0.15	-0.05
CDD	0.09	0.16	0.44	-0.15	0.44	1	0.01	0.21	-0.19	-0.12	-0.24
SU	-0.12	-0.16	-0.21	-0.35	0.10	0.01	1	0.20	0.12	0.32	0.22
TNx	0.07	0.00	0.23	0.08	-0.11	0.21	0.20	1	-0.10	-0.22	0.02
TXx	0.04	0.23	0.00	0.05	0.00	-0.19	0.12	-0.10	1	-0.19	0.01
TXn	0.28	0.03	-0.03	0.13	0.15	-0.12	0.32	-0.22	-0.19	1	0.31
TNn	0.04	0.17	-0.01	0.10	-0.05	-0.24	0.22	0.02	0.01	0.31	1

Indices (CNRM-CM5)	PRCPTOT	SDII	R95PTOT	R99PTOT	CWD	CDD	SU	TNx	TXx	TXn	TNn
PRCPTOT	1	0.57	0.22	0.16	0.30	0.09	0.08	0.28	0.07	0.60	0.41
SDII	0.57	1	0.35	0.35	0.37	0.39	-0.26	0.50	0.55	0.29	0.32
R95PTOT	0.22	0.35	1	0.25	0.22	-0.16	-0.37	0.18	0.54	-0.07	-0.02
R99PTOT	0.16	0.35	0.25	1	0.13	0.16	0.18	0.41	0.51	0.32	0.41
CWD	0.30	0.37	0.22	0.13	1	0.50	-0.33	0.22	0.24	0.02	0.06
CDD	0.09	0.39	-0.16	0.16	0.50	1	-0.24	0.44	0.26	-0.14	0.11
SU	0.08	-0.26	-0.37	0.18	-0.33	-0.24	1	0.07	-0.34	0.63	0.28
TNx	0.28	0.50	0.18	0.41	0.22	0.44	0.07	1	0.14	0.20	0.18
TXx	0.07	0.55	0.54	0.51	0.24	0.26	-0.34	0.14	1	-0.12	0.19
TXn	0.60	0.29	-0.07	0.32	0.02	-0.14	0.63	0.20	-0.12	1	0.37
TNn	0.41	0.32	-0.02	0.41	0.06	0.11	0.28	0.18	0.19	0.37	1

Indices (CCSM4)	PRCPTOT	SDII	R95PTOT	R99PTOT	CWD	CDD	SU	TNx	TXx	TXn	TNn
PRCPTOT	1	0.64	0.01	0.41	-0.15	-0.03	0.03	0.18	0.26	0.49	-0.06
SDII	0.64	1	0.39	0.57	0.40	0.30	-0.11	0.45	0.51	0.11	-0.13
R95PTOT	0.01	0.39	1	0.38	0.36	0.24	-0.18	0.17	0.15	-0.15	-0.18
R99PTOT	0.41	0.57	0.38	1	-0.14	-0.10	-0.16	0.13	0.19	0.21	0.05
CWD	-0.15	0.40	0.36	-0.14	1	0.55	-0.03	0.26	-0.02	-0.35	0.00
CDD	-0.03	0.30	0.24	-0.10	0.55	1	0.24	0.46	-0.13	-0.19	-0.19
SU	0.03	-0.11	-0.18	-0.16	-0.03	0.24	1	-0.11	-0.34	0.28	0.08
TNx	0.18	0.45	0.17	0.13	0.26	0.46	-0.11	1	0.37	0.14	0.14
TXx	0.26	0.51	0.15	0.19	-0.02	-0.13	-0.34	0.37	1	-0.10	0.07
TXn	0.49	0.11	-0.15	0.21	-0.35	-0.19	0.28	0.14	-0.10	1	0.18
TNn	-0.06	-0.13	-0.18	0.05	0.00	-0.19	0.08	0.14	0.07	0.18	1

**Table 4.** Correlation matrix of 11 climate indices using five GCMs during the future period (2040-2059).

Indices (BCC-CSM1.1)	PRCPTOT	SDII	R95PTOT	R99PTOT	CWD	CDD	SU	TNx	TXx	TXn	TNn
PRCPTOT	1	0.59	0.46	0.17	0.18	-0.48	-0.29	0.02	0.13	-0.22	0.42
SDII	0.59	1	0.44	0.44	0.07	-0.26	0.07	0.08	0.48	0.08	0.67
R95PTOT	0.46	0.44	1	0.30	0.30	-0.33	0.26	0.32	0.35	-0.03	0.38
R99PTOT	0.17	0.44	0.30	1	-0.08	-0.20	0.02	0.55	0.58	-0.12	0.18
CWD	0.18	0.07	0.30	-0.08	1	0.21	-0.05	-0.09	0.03	0.06	-0.11
CDD	-0.48	-0.26	-0.33	-0.20	0.21	1	0.22	-0.34	-0.13	0.33	-0.25
SU	-0.29	0.07	0.26	0.02	-0.05	0.22	1	0.28	0.02	0.17	0.31
TNx	0.02	0.08	0.32	0.55	-0.09	-0.34	0.28	1	0.48	0.09	0.14
TXx	0.13	0.48	0.35	0.58	0.03	-0.13	0.02	0.48	1	0.12	0.36
TXn	-0.22	0.08	-0.03	-0.12	0.06	0.33	0.17	0.09	0.12	1	0.18
TNn	0.42	0.67	0.38	0.18	-0.11	-0.25	0.31	0.14	0.36	0.18	1

Indices (MRI-CGCM3)	PRCPTOT	SDII	R95PTOT	R99PTOT	CWD	CDD	SU	TNx	TXx	TXn	TNn
PRCPTOT	1	0.09	0.16	0.32	-0.41	0.04	0.06	0.12	0.18	0.22	-0.20
SDII	0.09	1	0.16	0.19	-0.14	-0.13	-0.14	0.29	0.28	-0.18	-0.03
R95PTOT	0.16	0.16	1	0.17	0.03	-0.51	-0.02	0.22	0.09	-0.06	0.32
R99PTOT	0.32	0.19	0.17	1	0.03	-0.10	0.20	-0.01	-0.13	0.25	-0.02
CWD	-0.41	-0.14	0.03	0.03	1	0.31	0.08	0.07	-0.09	0.06	0.25
CDD	0.04	-0.13	-0.51	-0.10	0.31	1	0.11	-0.07	-0.06	0.30	-0.08
SU	0.06	-0.14	-0.02	0.20	0.08	0.11	1	0.30	-0.12	0.78	0.43
TNx	0.12	0.29	0.22	-0.01	0.07	-0.07	0.30	1	0.18	-0.01	0.11
TXx	0.18	0.28	0.09	-0.13	-0.09	-0.06	-0.12	0.18	1	-0.14	-0.02
TXn	0.22	-0.18	-0.06	0.25	0.06	0.30	0.78	-0.01	-0.14	1	0.27
TNn	-0.20	-0.03	0.32	-0.02	0.25	-0.08	0.43	0.11	-0.02	0.27	1

Indices (GISS-E2R)	PRCPTOT	SDII	R95PTOT	R99PTOT	CWD	CDD	SU	TNx	TXx	TXn	TNn
PRCPTOT	1	0.26	0.36	0.42	-0.19	0.05	-0.10	0.40	0.02	0.26	0.32
SDII	0.26	1	0.18	0.55	0.34	-0.03	0.02	0.15	0.42	0.34	0.21
R95PTOT	0.36	0.18	1	0.36	0.24	0.44	-0.27	0.23	0.05	-0.03	0.20
R99PTOT	0.42	0.55	0.36	1	0.19	-0.18	-0.31	0.14	0.20	0.11	-0.02
CWD	-0.19	0.34	0.24	0.19	1	0.35	0.01	-0.13	-0.04	0.12	-0.23
CDD	0.05	-0.03	0.44	-0.18	0.35	1	-0.16	0.20	-0.31	-0.08	-0.23
SU	-0.10	0.02	-0.27	-0.31	0.01	-0.16	1	0.29	0.10	0.30	0.13
TNx	0.40	0.15	0.23	0.14	-0.13	0.20	0.29	1	-0.30	0.15	0.08
TXx	0.02	0.42	0.05	0.20	-0.04	-0.31	0.10	-0.30	1	-0.07	0.26
TXn	0.26	0.34	-0.03	0.11	0.12	-0.08	0.30	0.15	-0.07	1	0.20
TNn	0.32	0.21	0.20	-0.02	-0.23	-0.23	0.13	0.08	0.26	0.20	1

Indices (CNRM-CM5)	PRCPTOT	SDII	R95PTOT	R99PTOT	CWD	CDD	SU	TNx	TXx	TXn	TNn
PRCPTOT	1	0.40	0.12	0.13	0.27	0.09	0.16	0.14	-0.22	0.61	0.18
SDII	0.40	1	0.21	0.33	0.18	0.20	-0.12	0.15	0.31	0.27	0.01
R95PTOT	0.12	0.21	1	0.32	0.15	-0.26	-0.35	0.34	0.46	-0.04	-0.16
R99PTOT	0.13	0.33	0.32	1	0.15	0.06	0.27	0.32	0.34	0.17	0.30
CWD	0.27	0.18	0.15	0.15	1	0.43	-0.21	0.16	0.13	0.31	-0.17
CDD	0.09	0.20	-0.26	0.06	0.43	1	-0.28	0.06	0.28	-0.09	0.08
SU	0.16	-0.12	-0.35	0.27	-0.21	-0.28	1	-0.08	-0.51	0.51	0.31
TNx	0.14	0.15	0.34	0.32	0.16	0.06	-0.08	1	0.16	-0.05	0.42
TXx	-0.22	0.31	0.46	0.34	0.13	0.28	-0.51	0.16	1	-0.38	0.12
TXn	0.61	0.27	-0.04	0.17	0.31	-0.09	0.51	-0.05	-0.38	1	-0.02
TNn	0.18	0.01	-0.16	0.30	-0.17	0.08	0.31	0.42	0.12	-0.02	1

Indices (CCSM4)	PRCPTOT	SDII	R95PTOT	R99PTOT	CWD	CDD	SU	TNx	TXx	TXn	TNn
PRCPTOT	1	0.48	0.02	0.41	-0.06	-0.06	0.09	0.27	0.22	<b>0.51</b>	-0.02
SDII	0.48	1	0.32	0.34	0.59	0.40	0.09	0.38	0.22	0.42	-0.41
R95PTOT	0.02	0.32	1	0.38	0.55	0.26	-0.16	0.09	0.12	0.02	-0.35
R99PTOT	0.41	0.34	0.38	1	0.03	-0.14	0.12	0.17	0.26	0.10	0.01
CWD	-0.06	0.59	0.55	0.03	1	0.65	0.13	0.06	-0.12	0.00	-0.38
CDD	-0.06	0.40	0.26	-0.14	0.65	1	0.23	0.23	0.14	-0.11	-0.41
SU	0.09	0.09	-0.16	0.12	0.13	0.23	1	0.07	-0.33	-0.01	0.01
TNx	0.27	0.38	0.09	0.17	0.06	0.23	0.07	1	0.30	0.40	-0.07
TXx	0.22	0.22	0.12	0.26	-0.12	0.14	-0.33	0.30	1	0.04	-0.06
TXn	0.51	0.42	0.02	0.10	0.00	-0.11	-0.01	0.40	0.04	1	-0.03
TNn	-0.02	-0.41	-0.35	0.01	-0.38	-0.41	0.01	-0.07	-0.06	-0.03	1

**Table 5.** Correlation matrix of 11 climate indices using five GCMs during the future period (2060-2079).

Indices (BCC-CSM1.1)	PRCPTOT	SDII	R95PTOT	R99PTOT	CWD	CDD	SU	TNx	TXx	TXn	TNn
PRCPTOT	1	0.61	0.53	0.22	0.21	-0.47	-0.08	0.12	0.16	0.01	0.42
SDII	0.61	1	0.42	0.51	-0.19	-0.28	0.08	0.39	0.49	0.12	0.52
R95PTOT	0.53	0.42	1	0.30	0.34	-0.31	0.24	0.20	0.27	0.10	0.34
R99PTOT	0.22	0.51	0.30	1	-0.09	-0.20	0.03	0.64	0.22	-0.07	0.11
CWD	0.21	-0.19	0.34	-0.09	1	0.06	0.04	-0.01	0.22	0.00	-0.14
CDD	-0.47	-0.28	-0.31	-0.20	0.06	1	0.21	-0.23	0.23	0.23	-0.19
SU	-0.08	0.08	0.24	0.03	0.04	0.21	1	0.36	0.31	0.52	0.29
TNx	0.12	0.39	0.20	0.64	-0.01	-0.23	0.36	1	0.14	0.40	0.27
TXx	0.16	0.49	0.27	0.22	0.22	0.23	0.31	0.14	1	0.27	0.16
TXn	0.01	0.12	0.10	-0.07	0.00	0.23	0.52	0.40	0.27	1	0.33
TNn	0.42	0.52	0.34	0.11	-0.14	-0.19	0.29	0.27	0.16	0.33	1

Indices (MRI-CGCM3)	PRCPTOT	SDII	R95PTOT	R99PTOT	CWD	CDD	SU	TNx	TXx	TXn	TNn
PRCPTOT	1	0.14	0.09	0.29	-0.28	0.08	0.13	0.03	0.20	0.12	-0.04
SDII	0.14	1	0.02	0.29	-0.15	-0.02	0.22	-0.12	0.33	0.08	-0.21
R95PTOT	0.09	0.02	1	0.16	0.10	-0.51	-0.15	0.06	0.24	0.16	0.61
R99PTOT	0.29	0.29	0.16	1	0.04	-0.07	0.30	-0.23	0.14	0.30	0.05
CWD	-0.28	-0.15	0.10	0.04	1	0.37	0.07	0.22	-0.06	0.12	0.13
CDD	0.08	-0.02	-0.51	-0.07	0.37	1	0.19	0.05	-0.24	0.18	-0.27
SU	0.13	0.22	-0.15	0.30	0.07	0.19	1	0.07	-0.13	0.70	0.34
TNx	0.03	-0.12	0.06	-0.23	0.22	0.05	0.07	1	-0.25	0.05	0.11
TXx	0.20	0.33	0.24	0.14	-0.06	-0.24	-0.13	-0.25	1	-0.02	-0.23
TXn	0.12	0.08	0.16	0.30	0.12	0.18	0.70	0.05	-0.02	1	0.36
TNn	-0.04	-0.21	0.61	0.05	0.13	-0.27	0.34	0.11	-0.23	0.36	1

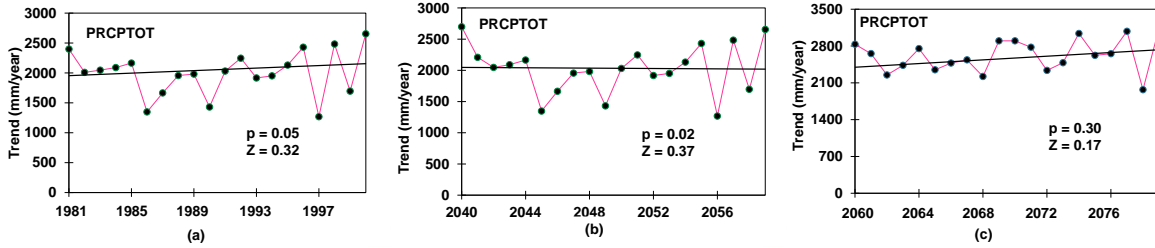
Indices (GISS-E2R)	PRCPTOT	SDII	R95PTOT	R99PTOT	CWD	CDD	SU	TNx	TXx	TXn	TNn
PRCPTOT	1	0.21	0.47	0.32	0.08	0.24	-0.13	0.32	0.02	0.20	0.28
SDII	0.21	1	0.04	0.51	0.24	-0.17	0.13	0.18	0.26	0.48	0.19
R95PTOT	0.47	0.04	1	0.43	0.18	0.37	-0.41	0.27	0.22	-0.02	0.10
R99PTOT	0.32	0.51	0.43	1	0.15	0.01	-0.35	0.08	0.28	-0.03	0.14
CWD	0.08	0.24	0.18	0.15	1	0.27	0.00	-0.15	-0.04	0.31	-0.18
CDD	0.24	-0.17	0.37	0.01	0.27	1	-0.21	0.25	-0.24	0.01	-0.27
SU	-0.13	0.13	-0.41	-0.35	0.00	-0.21	1	0.07	0.00	0.50	0.13
TNx	0.32	0.18	0.27	0.08	-0.15	0.25	0.07	1	-0.32	0.11	-0.05
TXx	0.02	0.26	0.22	0.28	-0.04	-0.24	0.00	-0.32	1	-0.20	0.35
TXn	0.20	0.48	-0.02	-0.03	0.31	0.01	0.50	0.11	-0.20	1	0.18
TNn	0.28	0.19	0.10	0.14	-0.18	-0.27	0.13	-0.05	0.35	0.18	1

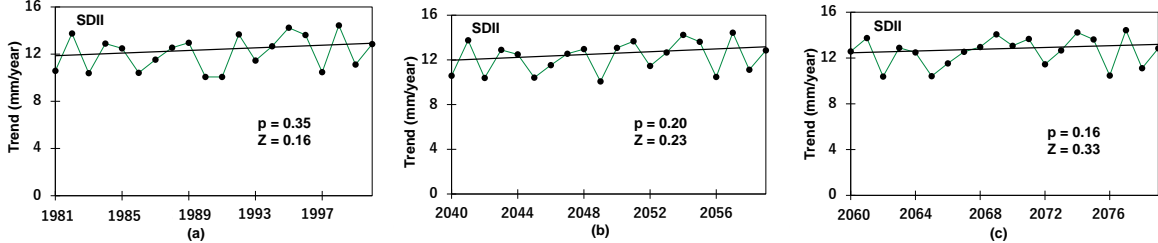
Indices (CNRM-CM5)	PRCPTOT	SDII	R95PTOT	R99PTOT	CWD	CDD	SU	TNx	TXx	TXn	TNn
PRCPTOT	1	0.22	0.04	0.10	0.23	-0.04	0.22	0.36	-0.24	0.52	0.13
SDII	0.22	1	0.32	0.64	0.03	-0.17	0.10	0.20	0.11	0.20	0.18
R95PTOT	0.04	0.32	1	0.33	0.16	0.01	-0.34	0.16	0.43	0.33	-0.20
R99PTOT	0.10	0.64	0.33	1	0.15	0.08	0.12	0.37	0.39	0.30	0.29
CWD	0.23	0.03	0.16	0.15	1	0.27	-0.17	0.35	0.23	0.22	-0.23
CDD	-0.04	-0.17	0.01	0.08	0.27	1	-0.47	-0.11	0.46	-0.31	0.16
SU	0.22	0.10	-0.34	0.12	-0.17	-0.47	1	0.35	-0.28	0.28	0.16
TNx	0.36	0.20	0.16	0.37	0.35	-0.11	0.35	1	-0.02	0.43	0.12
TXx	-0.24	0.11	0.43	0.39	0.23	0.46	-0.28	-0.02	1	0.02	0.02
TXn	0.52	0.20	0.33	0.30	0.22	-0.31	0.28	0.43	0.02	1	-0.41
TNn	0.13	0.18	-0.20	0.29	-0.23	0.16	0.16	0.12	0.02	-0.41	1

Indices (CCSM4)	PRCPTOT	SDII	R95PTOT	R99PTOT	CWD	CDD	SU	TNx	TXx	TXn	TNn
PRCPTOT	1	0.43	0.04	0.41	-0.18	-0.05	0.19	-0.18	0.03	0.52	0.20
SDII	0.43	1	0.06	0.46	0.15	0.12	-0.03	0.01	0.59	0.43	0.11
R95PTOT	0.04	0.06	1	0.39	0.38	0.25	-0.14	-0.21	-0.07	0.27	-0.60
R99PTOT	0.41	0.46	0.39	1	-0.14	-0.07	0.16	0.08	0.36	0.31	-0.07
CWD	-0.18	0.15	0.38	-0.14	1	0.60	-0.19	-0.44	-0.14	-0.07	-0.54
CDD	-0.05	0.12	0.25	-0.07	0.60	1	0.09	-0.08	0.03	0.09	-0.32
SU	0.19	-0.03	-0.14	0.16	-0.19	0.09	1	0.35	-0.21	0.15	0.40
TNx	-0.18	0.01	-0.21	0.08	-0.44	-0.08	0.35	1	0.18	0.20	0.36
TXx	0.03	0.59	-0.07	0.36	-0.14	0.03	-0.21	0.18	1	-0.08	0.26
TXn	0.52	0.43	0.27	0.31	-0.07	0.09	0.15	0.20	-0.08	1	-0.07
TNn	0.20	0.11	-0.60	-0.07	-0.54	-0.32	0.40	0.36	0.26	-0.07	1



**Fig. 5.** Trend magnitudes of PRCPTOT indices at Bago Station during (a) past period (1981-2000), (b) future period (2040-2059) and (c) future period (2060-2079).



**Fig. 6.** Trend magnitudes of SDII indices at Bago Station during (a) past period (1981-2000), (b) future period (2040-2059) and (c) future period (2060-2079).

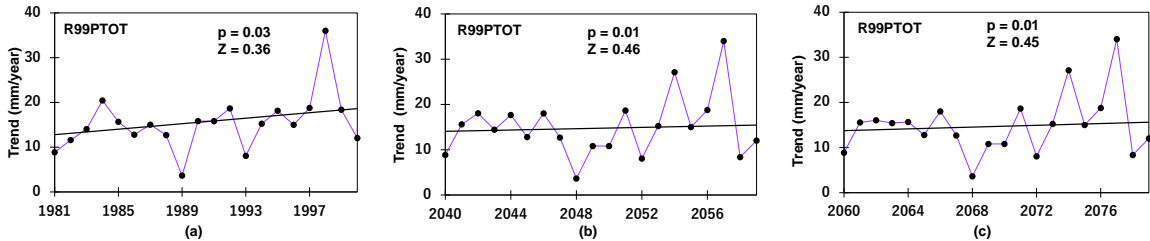


**Fig. 7.** Trend magnitudes of R99PTOT indices at Bago Station during (a) past period (1981-2000), (b) future period (2040-2059) and (c) future period (2060-2079).

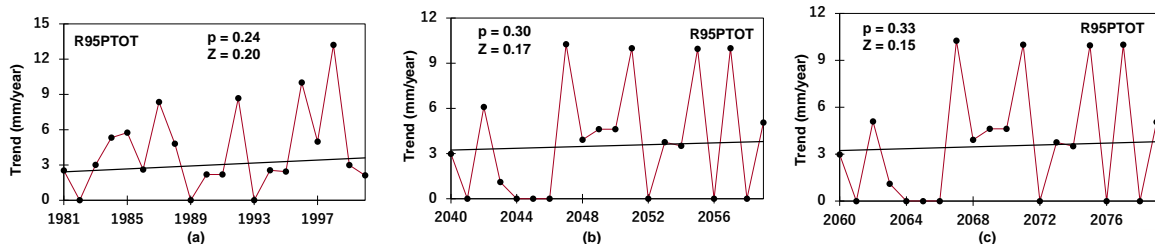


**Fig. 8.** Trend magnitudes of R95PTOT indices at Bago Station during (a) past period (1981-2000), (b) future period (2040-2059) and (c) future period (2060-2079).

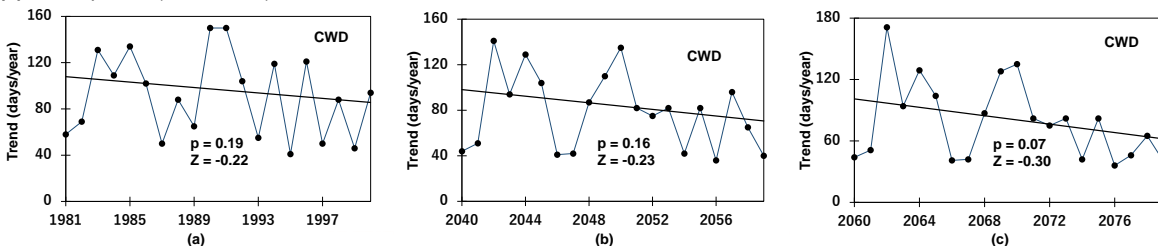


**Fig. 9.** Trend magnitudes of CWD indices at Bago Station during (a) past period (1981-2000), (b) future period (2040-2059) and (c) future period (2060-2079).

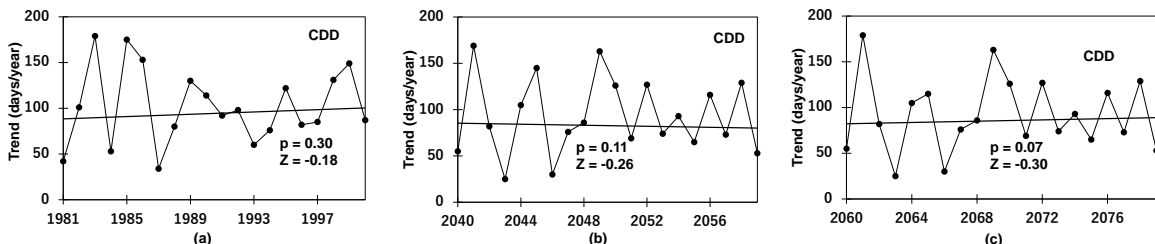


**Fig. 10.** Trend magnitudes of CDD indices at Bago Station during (a) past period (1981-2000), (b) future period (2040-2059) and (c) future period (2060-2079).

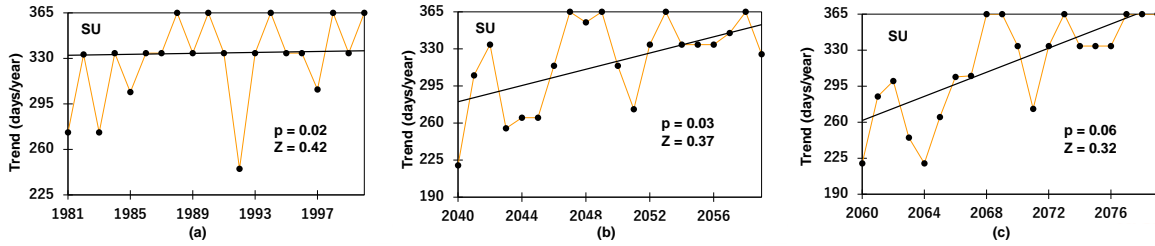


**Fig. 11.** Trend magnitudes of SU indices at Bago Station during (a) past period (1981-2000), (b) future period (2040-2059) and (c) future period (2060-2079).

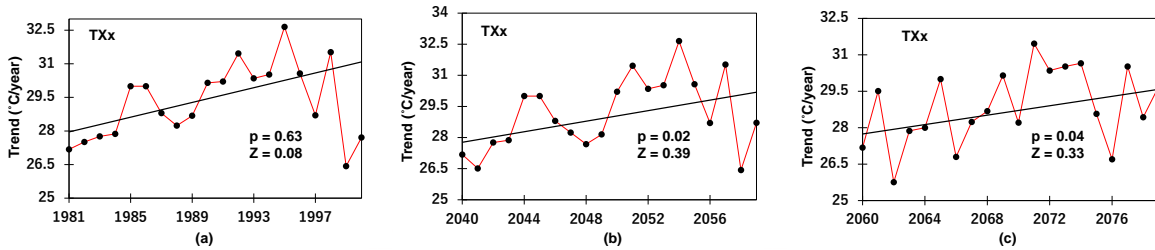


**Fig. 12.** Trend magnitudes of TXx indices at Bago Station during (a) past period (1981-2000), (b) future period (2040-2059) and (c) future period (2060-2079).

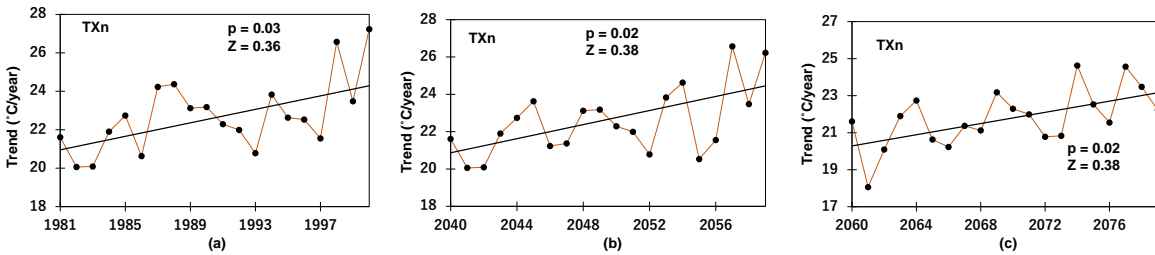


**Fig. 13.** Trend magnitudes of TXn indices at Bago Station during (a) past period (1981-2000), (b) future period (2040-2059) and (c) future period (2060-2079).

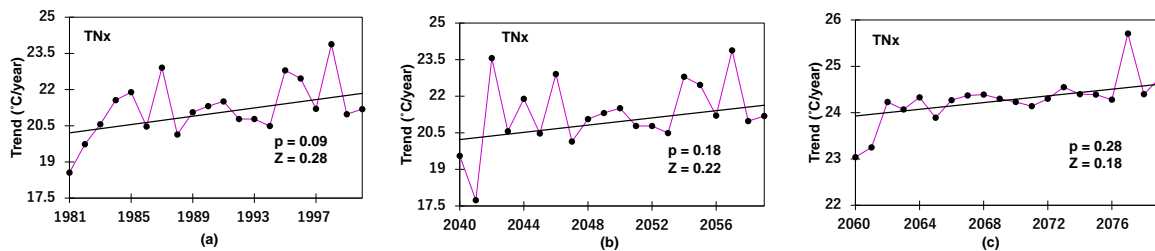


**Fig. 14.** Trend magnitudes of TNx indices at Bago Station during (a) past period (1981-2000), (b) future period (2040-2059) and (c) future period (2060-2079).

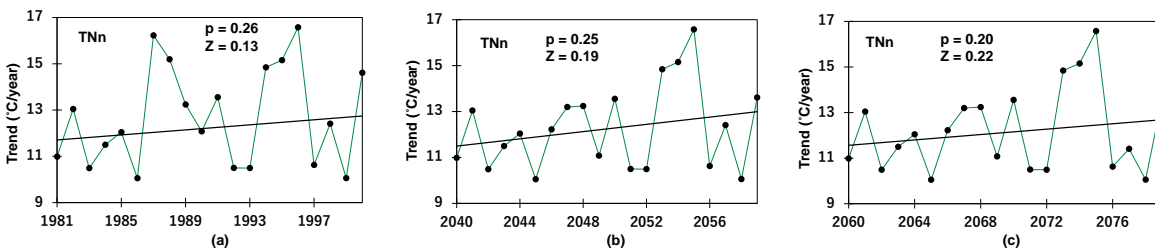


**Fig. 15.** Trend magnitudes of TNn indices at Bago Station during (a) past period (1981-2000), (b) future period (2040-2059) and (c) future period (2060-2079).

4.2.2 Temperature

In terms of temperature indices, every index indicates that maximum value of daily maximum temperature and maximum value of daily minimum temperatures are continually warming for future. Table 3, Table 4 and Table 5 mention the correlation matrices of each climate indices related to temperature and precipitation variables in time series scale. The annual maximum values of the daily minimum temperature (TNx) and the annual maximum value of daily maximum temperature (TXx) display strong correlations at Bago Station during the number of summer days (SU) that when daily maximum temperature is greater than 25°C in the past period (1981-2000).

In order to investigate the significant trend of temperature and precipitation in the Bago River Basin, Myanmar, the MK test and p-value test have been applied. The positive Kendall's Z values indicate an upward tendency and suggest that this trend will continue over time. Figure 11 mention the SU's upward future trend. It means that there will be an increase in the number of summer days, which will cause this basin to warm. According to analysis, the annual maximum temperature values of the daily maximum temperature (TXx) and the annual minimum temperature values of the daily maximum temperature (TXn) climate indices exhibit the upward tendency in both future time periods (Figure 12 and Figure 13). Furthermore, the TNx index has been showing an increasing trend during the past and future periods and the TNn index as well (Figure 14 and Figure 15). According to these findings, temperatures have been increasing for future periods compared to the past 20 years.

4.3 Evaluation of Hydrological Components

The impact of climate change on water balance was evaluated using the GCMs under the RCP 4.5 scenario. The average annual water balance components including the surface flow, lateral flow, groundwater flow and evapotranspiration related to five different GCMs during the past period (1981-2000) are shown in Figure 16 (a). In the past period, the average annual surface flow has increased by 30% in BCC-CSM1.1, 32% in MRI-CGCM3, 29% in GISS-E2R, 28% in CNRM-CM5, and 27% in CCSM4, according to each of models' performance. In addition, each GCM shows a significant increase in the percentage changes in average annual evapotranspiration throughout the past years. However, the percent change in average annual lateral flow is not particularly distinct between the observed and GCMs data. In contrast to the aforementioned five GCMs, CNRM-CM5 has the fewest deviations from the observed data. Figure 16 (b) and Figure 16 (c) show the percent change of

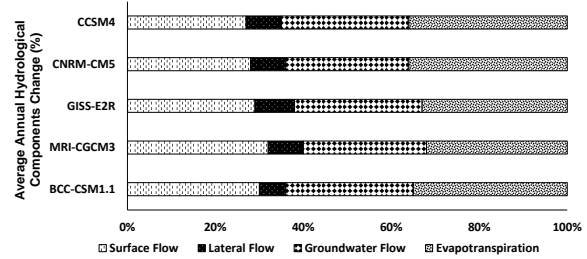


Fig. 16 (a). Average annual water balance components change in % using five GCMs during the past period (1981-2000).

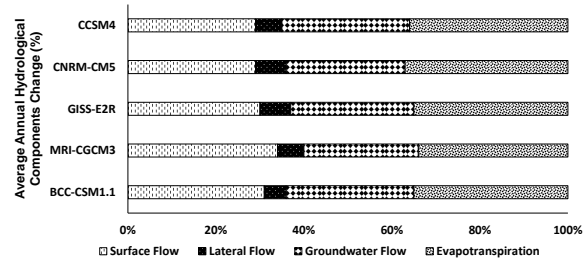


Fig. 16 (b). Average annual water balance components change in % using five GCMs during the future period (2040-2059).

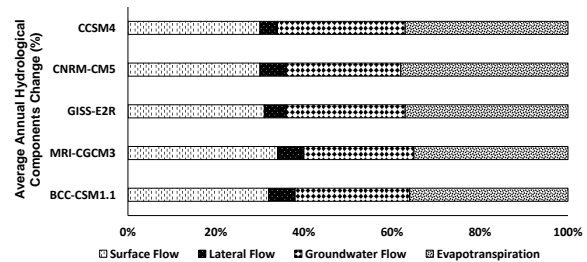


Fig. 16 (c). Average annual water balance components change in % using five GCMs during the future period (2060-2079).

average annual hydrological components using multiple GCMs for the future periods (2040-2059 and 2060-2079), respectively, under the RCP 4.5 scenario. In general, it is feasible to predict that all aspects of water balance components will alter substantially over the period of 2060-2079 compared to the period of 2040-2059. The average annual surface flow and evapotranspiration are also expected to be higher than the past period.

Figure 17 expressed the annual surface flow variability using 11 climate indices for both the past and the future periods. According to this graph (Figure 17), the surface flow will consistently rise across all subsequent time periods. In comparison to other climate indices throughout three different time periods, surface flow utilizing the PRCPTOT indicator has a substantial impact. The maximum value of the surface flow fluctuation for the annual total precipitation climate index (PRCPTOT) ranges from 1,694 mm/year in 2040-2059 to 1,986 mm/year in 2060-2079. The surface flow of water balance is directly impacted by the significant amount of precipitation. However, the annual lateral flow utilizing all

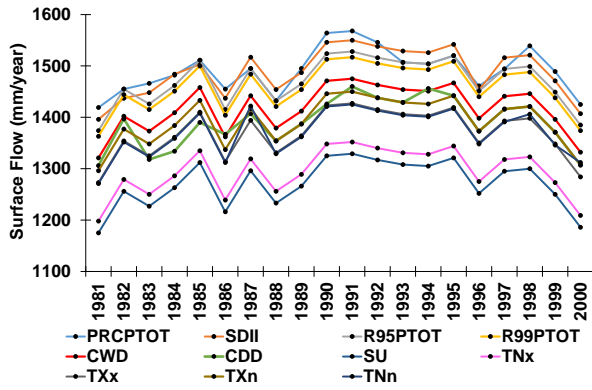


Fig. 17 (a). Annual surface flow variability by using 11 climate indices during the past period (1981-2000).

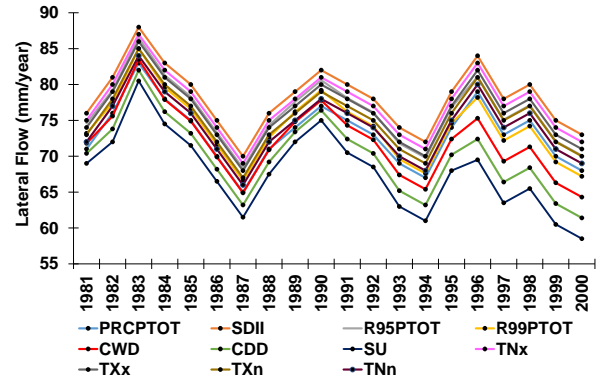


Fig. 18 (a). Annual lateral flow variability by using 11 climate indices during the past period (1981-2000).

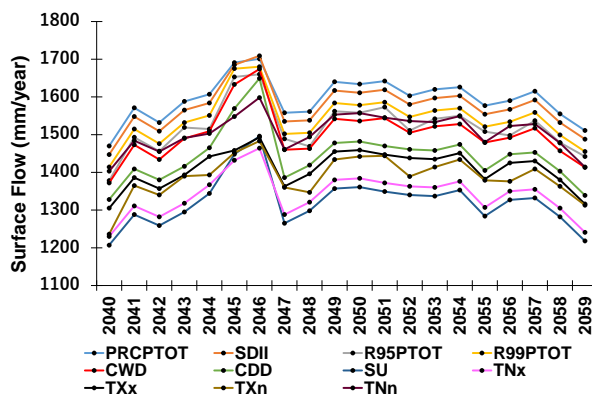


Fig. 17 (b). Annual surface flow variability by using 11 climate indices during the future period (2040-2059).

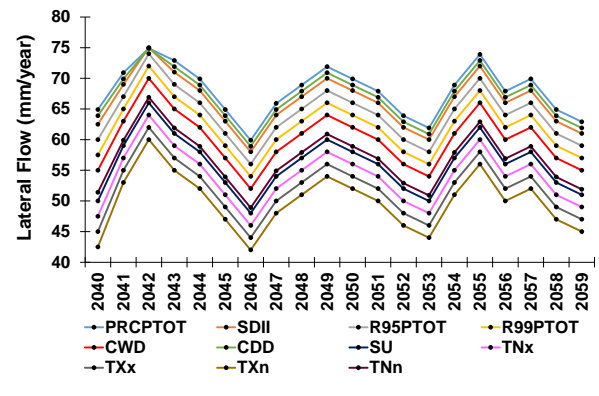


Fig. 18 (b). Annual lateral flow variability by using 11 climate indices during the future period (2040-2059).

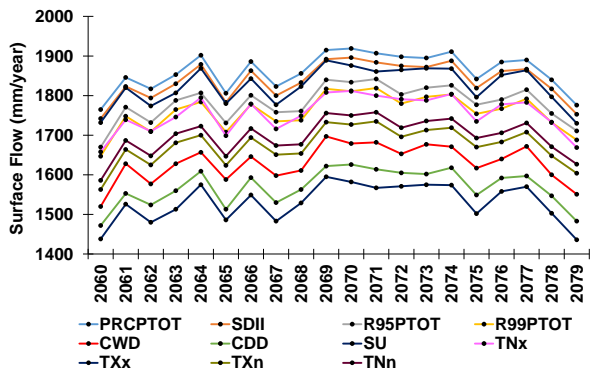


Fig. 17 (c). Annual surface flow variability by using 11 climate indices during the future period (2060-2079).

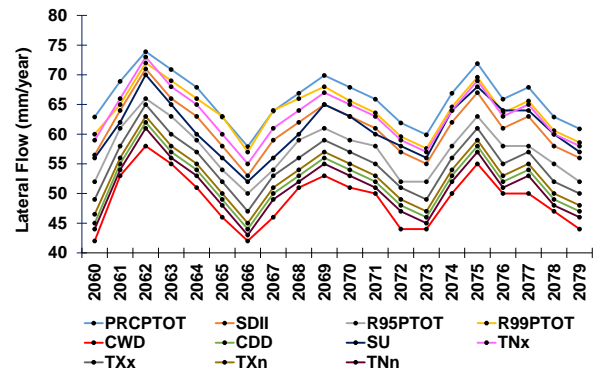


Fig. 18 (c). Annual lateral flow variability by using 11 climate indices during the future period (2060-2079).

climate indices will decline in both upcoming periods (Figure 18). Over two future periods, it is anticipated that there will be some fluctuation changes in the lateral flow using the precipitation climate indices (PRCPTOT, SDII, R95PTOT, R99PTOT, CWD, and CDD). On the other hand, the lateral flow utilizing the temperature indices (SU, TNx, TXx, TNn, and TXn) shows few differences in both the future periods compared to the past period.

Figure 19 demonstrates the annual variations of groundwater flow over the past and future periods. The groundwater flow will marginally rise in future times by employing the climate indices. Moreover, future extreme climatic indices will have an impact on the hydrological process due to the increase in evapotranspiration driven by the adoption of temperature indices (SU, TNx, TXx, TNn, and TXn) (Figure 20). In order to manage the water

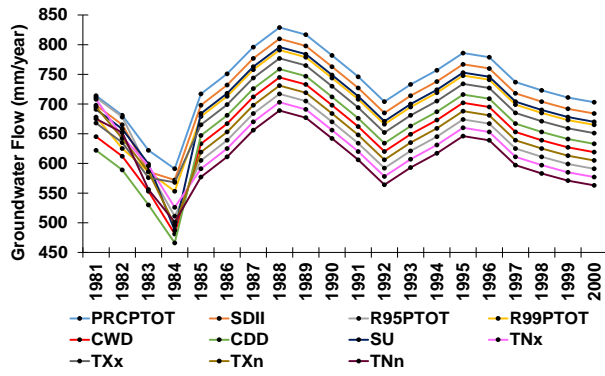


Fig. 19 (a). Annual groundwater flow variability by using 11 climate indices during the past period (1981-2000).

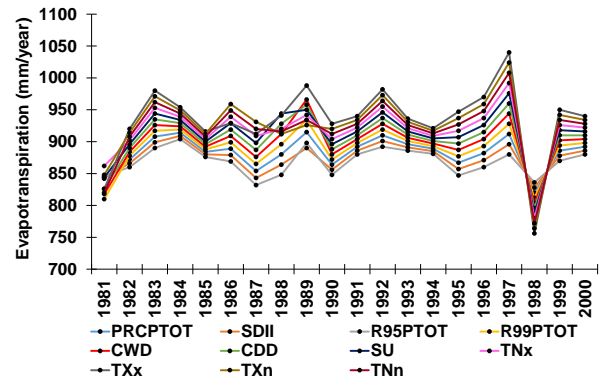


Fig. 20 (a). Annual evapotranspiration variability by using 11 climate indices during the past period (1981-2000).

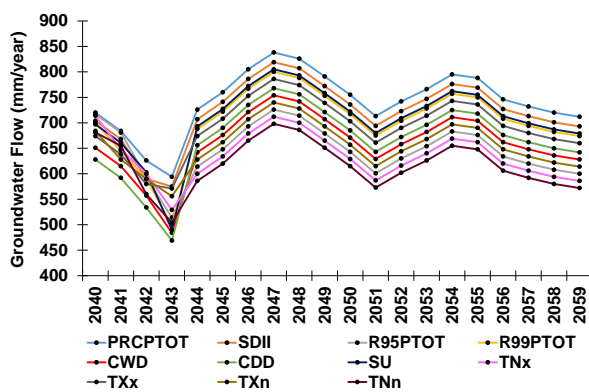


Fig. 19 (b). Annual groundwater flow variability by using 11 climate indices during the future period (2040-2059).

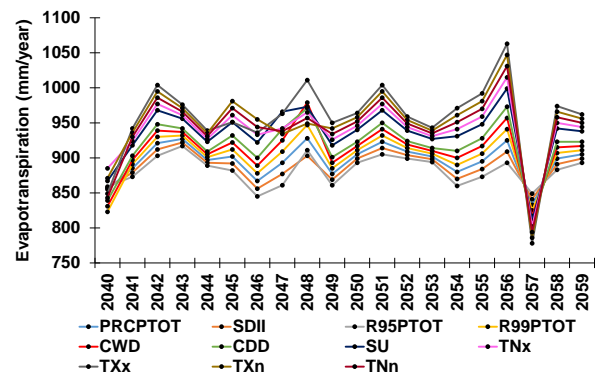


Fig. 20 (b). Annual evapotranspiration variability by using 11 climate indices during the future period (2040-2059).

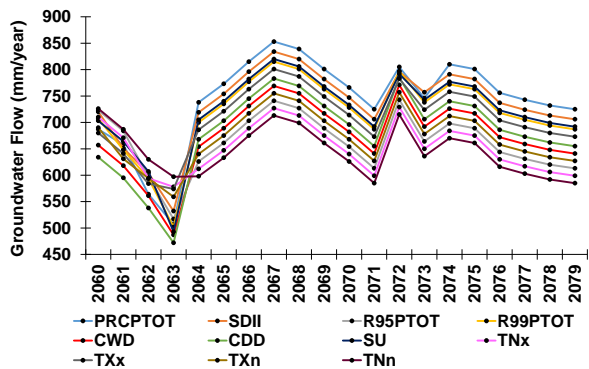


Fig. 19 (c). Annual lateral flow variability by using 11 climate indices during the future period (2060-2079).

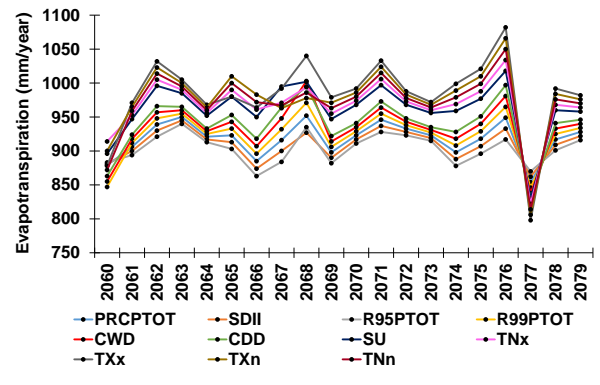


Fig. 20 (c). Annual evapotranspiration variability by using 11 climate indices during the future period (2060-2079).

resources in a watershed, it is essential to overcome how extreme climate change affects the hydrological process in the Bago River Basin, Myanmar.

### 5. Conclusions

This paper focuses on how the hydrological process of the Bago River Basin is affected by extreme climatic indices. According to the analysis's findings, the annual

total precipitation (PRCPTOT), precipitation intensity (SDII), and maximum temperature values in daily maximum temperature (TXx) indices will have a substantial impact on future periods. The water balance components of the Bago River Basin on the hydrological process are examined using the SWAT model to determine the effects of each extreme climate index alteration. The model is successfully constructed and

sufficiently operates to provide for an accurate analysis of the watershed using five different GCMs. Additionally, bias-corrected GCMs can be employed to evaluate the hydrological components, including the effects of climate change. Moreover, the surface flow will be more significant in magnitude and frequency under the RCP 4.5 scenario for all future periods. The evapotranspiration is also expected to increase as a result of the extremes temperature. Consequently, it is projected that both the groundwater flow and the lateral flow will decline in the coming years. Furthermore, there are other factors that contribute to hydrological process and the components of the water balance. Land use, land cover change and other aspects of the river system that are impacted by human effect also play an important role in such hydrological process and can be explored more as a result of these factors, which are excluded from the study. This paper examines the impact of extreme climatic indices on regional hydrological processes in the Bago River Basin for the future periods.

#### Acknowledgements

The authors are grateful to the Department of Meteorology and Hydrology in Myanmar for necessary data support such as rainfall, temperature and discharge data.

#### References

- Afzal, M., Gagnon, A. S., and Mansell, M. G., 2015. Changes in the variability and periodicity of precipitation in Scotland. *Theoretical and Applied Climatology*, 119: 135-159.
- Aguayo, R., Leon-Munoz, J., Garreaud, R. et al., 2021. Hydrological droughts in the Southern Andes (40-40S) form an ensemble experiment using CMIP5 and CMIP6 models. *Scientific Reports* 11, 5530.
- Ahmadalipour, A., Moradkhani, H., and Rana, A., 2018. Accounting for downscaling and model uncertainty in fine-resolution seasonal climate projections over the Columbia River Basin. *Climate Dynamics* 50, 717-733.
- Allen, S.K., Plattner, G. K., Nauels, A., Xin, Y. and Stocker, T. F., 2013. *Climate Change 2013: The Physical Science Basis. An overview of the Working Group 1 contribution to the Fifth Assessment Report of the Intergovernmental Panel on Climate Change (IPCC)*. Press United Kingdom, 2013, Cambridge University, New York, NY, USA: pp-1535.
- Aryal, J. P., Sapkota, T. B., and Khurana, R., 2020. Climate change agriculture in South Asia: adaptation options in smallholder production systems. *Environmental, Development and Sustainability* 22, 5045-5075.
- Benestad, R. E. 2004. Empirical-Statistical downscaling in Climate Modeling. *Earth Science and Applications from space*, 85 (42): 417-422.
- Brown, P. J., Bradley, R. S., and Keimig, F. T., 2010. Changes in extreme climate indices for the Northeastern United States, 1870-2005. *Journal of climate* 23, 6555-6572.
- Chen, H., Xu, C. Y., and Guo, S., 2012. Comparison and evaluation of multiple GCMs, statistical downscaling and hydrological models in the study of climate change impacts on runoff. *Journal of Hydrology*, Vol. 434, 2012, p. 36-45.
- Chapagain, D., Dhaubanjari, S., and Bharati, L., 2021. Unpacking future climate extremes and their sectoral implications in western Nepal. *Climate Change* 168, 8.
- Charles, B., Chisanga, A., Kabwe, H., Mubanga, B., et al., 2022. Modelling climatic trends for the Zambezi and Orange River Basins: implications on water security. *Journal of Water and Climate Change*, 00 (01), 1-22.
- Christensen, J. H., Boberg, F., Christensen, O. B., and Picher, P. L., 2008. On the need for bias correction of regional climate change projections of temperature and precipitation. *Geophysical Research Letters*, 35: 1-6.
- Coupled Model Intercomparison Project Phase 5 (CMIP5). <https://pcmdi.llnl.gov/mips/cmip5/>.
- Deser, C., Phillips, A., Bourdette, V., and Teng, H., 2012. Uncertainty in climate change projections: The role of internal variability. *Climate Dynamics* 38: 527-546.
- Dietzsch, F., Andersson, A., Ziese, M., Schroder, M., Raykova, K., Schamm, K., and Becker, A., 2017. A global ETCCDI-based precipitation climatology from satellite and rain gauge measurements. *Climate*, 17 (5): 9.
- Duhan, D., and Pandey, A., 2013. Statistical analysis of long term spatial and temporal trends of precipitation during 1901-2002 at Madhya Pradesh, India. *Atmospheric Research*, 122, 136-149.
- Felix, M. L., Kim, Y. K., Choi, M., et al., 2021. Detailed Trend Analysis of Extreme Climate Indices in the Upper Geum River Basin. *Water* 2021, 13, 3171.
- Gassman, P. W., Racher, M., 2007. The soil and water assessment tool: Historical development applications and future research directions. *Trans ASABE*, 50 (4): 1211-1250.
- Hirsch, R. M., Slack, J. R., and Smith, R. A., 1982. Techniques of trend analysis for monthly water quality data. *Water Resources Research*, 18: 107-121.
- Hlaing, K. W., Haruyama, S., and Aye, M. M., 2008. Using GIS-based distributed soil loss modeling and morphometric analysis to prioritize watershed for soil

- conservation in Bago river basin of Lower Myanmar. *Frontiers of Earth Science in China*, 2: 465-478.
- Htut, A. Y., Shrestha, S., Nitivattananon, V., and Kawasaki, A., 2014. Forecasting climate change scenarios in the Bago River Basin, Myanmar. *Journal of Earth Science and Climate Change* 5, 228.
- Htut, A. Y., 2015. Assessment of climate change and land use change impacts on the hydrology and water resources of the Bago River Basin in Myanmar. Ph.D Thesis, Asian Institute of Technology, Thailand.
- IPCC., 2001. Third Assessment Report, Working Group-I Report. Cambridge University Press, Cambridge, UK.
- Jose, D. M., and Dwarakish, G. G., 2022. Bias correction and trend analysis of temperature data by a high-resolution CMIP6 model over a tropical river basin. *Asia-Pacific Journal of Atmospheric Science* 58, 97-115.
- Kawasaki, A., Ichiharab, N., Ochiib, y., Aciertoc, R. A., Kodakad, A., and Zin, W. W., 2017. Disaster response and river infrastructure management during the 2015 Myanmar floods: A case in the Bago River Basin. *International Journal of Disaster Risk Reduction*, 24: 151-159.
- Kendall, M. G., 1975. Rank correlation methods. Oxford University Press, Oxford.
- Kundzewicz, Z. W., Krysanova, V., Benestad, R. E., Piniewski, M. and Otto, I. M., 2022. Uncertainty in climate change impacts on water resources. *Journal of Environmental Science*, 79: 1-8.
- Kyaw, T. O., 2022. Interannual variability of winter rainfall in Upper Myanmar. *Journal of Sustainability and Environmental Management (JOSEM)*, Vol. 1 (3), 344-358.
- Kyu, K. S., Chidthaisong, A., Pimple, U., Tin, M. H., and Varnakovida, P., 2016. Changes in temperature and precipitation and their extreme indices over Dry Zone Area in Central Myanmar. *International conference on Climate Change, Biodiversity and Ecosystem Services for the Sustainable Development Goals (SDGs): Policy and Practice*, 27-29 June 2016, Cha-Am, Phetchaburi, Thailand.
- Lenderink, G., Buishand, A., and Van, W., 2007. Estimates of future discharges of the river Rhine using two scenario methodologies: direct versus delta approach. *Hydrology and Earth System Science*, 11 (3): 1145-1159.
- Li, X., and Babovic, V., 2017. Analysis of variability and trends of precipitation extremes in Singapore during 1980-2013. *International Journal of Climatology*, 38: 125-141.
- Linlin, C., Changchun, X., Nanji, S., Lingling, S., and Xiaoni, L., 2023. Future dry-wet climatic characteristics and drought trends over arid Central Asia. *Frontiers in Earth Science*, Vol 11.
- Mishra, V., Bhatia, U., and Tiwari, A. D., 2020. Bias-corrected climate projections for South Asia from Coupled Model Intercomparison Project-6. *Scientific Data* 7, 228.
- Myo. H., Zin, W., Shwe, K., Kawasaki, A., and Acierto, R., 2020. Projecting the Impact of Climate Change on Temperature, Precipitation, and Discharge in the Bago River Basin. *Journal of Disaster Research*, Vol. 15 (3), 324-334.
- Nie, H., Qin, T., Yang, H., Chen, J., He, S., Lv, Z., and Shen, Z., 2019. Trend analysis of temperature and precipitation extremes during winter wheat growth period in the major winter wheat planting area of China. *Atmosphere*, 10: 240.
- Olsson, J., Arheimer, B., Borris, M., Donnelly, C., and Foster, K., 2016. Hydrological climate change impact assessment at small and large scales: Key messages from recent progress in Sweden. *Climate*, 4 (3): 39.
- Oruc, S., 2022. Performance of bias corrected monthly CMIP6 climate projections with different reference period data in Turkey. *Acta Geophysica*, Vol 70 (2), 777-789.
- Pat, J. F., and Wu, C., 2018. Recent acceleration of the Terrestrial hydrologic cycle in the U.S Midwest. *Advancing Earth and Space Science*, 123: 2993-3008.
- Pesce, M., Hardenberg, J. V., Claps e, P., and Viglione, A., 2022. Correlation between climate and flood indices in Northwestern Italy at different temporal scales. *Journal of Hydrology and Hydromechanics*, 70: 178-194.
- Raju, K. S. and Kumar, D. N., 2020. Review of approaches for selection and ensembling of GCMs. *Journal of Water and Climate Change*, 11 (3): 577-599.
- Rathjens, H., Bieger, K., Srinivasan, R., and Arnold, J. G., 2016. CMhyd user manual documentation for preparing simulated climate change data for hydrologic impact studies. *CMhyd User manual*, Texas.
- Rauscher, S. A., Erika, C., Claudio, P., and Filippo, G., 2013. Resolution effects on regional climate model simulations of seasonal precipitation over Europe. *ARGIS*, 35: 685-711.
- Sardella, A., Palazzi, E., Hardengerg, J. V., Grande, C. D., Nuntiis, R. D., Sabbioni, C., and Bonazza, A., 2020. Risk mapping for the sustainable protection of cultural heritage in extreme changing environments. *Journal of Atmosphere*, 11 (7): 700.
- Sein, K. K., Chidthaisong, A.; Oo, K.L., 2018. Observed Trends and Changes in Temperature and

- Precipitation Extreme Indices over Myanmar. *Atmosphere* 9, 477.
- Shelly, W., and Zin, W. W., 2014. Development of flood inundation map for the Bago river. Master thesis, Yangon Technological University, Yangon, Myanmar.
- Shelly, W., Zin, W. W., and Kawasaki, A., 2020. Development of Flood Damage Estimation Model for Agriculture – Case Study in the Bago Floodplain, Myanmar. *Journal of Disaster Risk Reduction*, 15 (3): 242-255.
- Shrestha, M., Shrestha, S., and Datta, A., 2014. Impact of climate change on the hydrology of upper Bago River Basin, Myanmar. *International Symposium on Environmental Flow and Water Resources Management*, October, 2014, Asian Institute of Technology, Thailand.
- Shrestha, S., and Htut, A. Y., 2016. Land use and climate change impacts on the hydrology of the Bago River Basin, Myanmar. *Environmental Model Assess* 21, 819-833.
- Shrestha, M., Shrestha, S., and Datta, A., 2017. Assessment of climate change impact on water diversion from the Bago River Basin to the Moyingyi wetland, Myanmar. *Current Science*, 112 (2), 377-384.
- Silva, M. G. D., Netto, A. O. A., Neves, R. J. J., Vasco, A. N., Almeida, C., and Faccioli, G. G., 2015. Sensitivity analysis and calibration of hydrological modeling of the watershed northeast Brazil. *Journal of Environmental Protection*, 6 (8): 837-850.
- Singh, V., and Goyal, M. K., 2016. Analysis and trends ices over north Sikkim eastern Himalayas under CMIPESM-2M RCPs experiments. *Atmospheric Research*, 167: 34-60.
- Singh, P. K., and Jain, S. K., 2019. Inter-comparisons CMs and statistically downscaled NEX-GDDP based precipitation in India. *Science of the total environment*, 697: 134163.
- Song, Y. H., Chung, E. S., and Shiru, M. S., 2020. Uncertainty analysis of monthly precipitation in GCMs using multiple bias correction methods under different RCPs. *Journal of Sustainability*, 12(18): 7508.
- Song, Y. H., Chung, E. S., and Shahid, S., 2022. The new bias correction method for daily extremes precipitation over South Korea using CMIP6 GCMs. *Journal of Water Resources Management* 36, 5977-5997.
- Taylor, K. E., Stouffer, R. J., and Meehl, G. A., 2012. An overview of CMIP 5 and the experiment design. *Bulletin of the American Meteorological Society*, 93: 485-498.
- Teutschbein, C., and Seibert, J., 2010. Regional climate models for hydrological impact studies at the catchment scale: a review of recent modeling strategies. *Geography Compass*, 4 (7): 834-860.
- Yacoub, E., and Tayfur, G., 2019. Trend analysis of temperature and precipitation in Trarza region of Mauritania. *Journal of Water and Climate Change*, 10 (3), 484-493.
- Yang, Y., and Tang, J., 2023. Downscaling and uncertainty analysis of future concurrent long-duration dry and hot events in China. *Journal of Climate Change* 176, 11.
- Yeboah, K. F., Akpoti, K., Kabobah, A. T., Oforu, E. A., Siabi, E. A., Mortey, E. M., and Okyereh, S. A., 2022. Assessing climate change projections in the Volta basin using the CORDEX-Africa climate simulations and statistical bias correction. *Environmental challenges*, 6: 100439.
- Zhang, X., Hegerl, G., Zwiers, F. W., and Kenyon, J., 2005. Avoiding inhomogeneity in percentile-based indices of temperature extremes. *Journal of climate*, 18:1641-1651.
- Zhang, X., Alexander, L., Hegerl, G. C., Jones, P., Tank, A. A., Peterson, T. C., Trewin, B., and Zwiers, F. W., 2011. Indices for monitoring changes in extremes based on daily temperature and precipitation data. *Wiley Interdisciplinary Reviews, Climate Change*, 2 (6): 851-870.
- Zwiers, F. W., and Zhang, X., 2009. Guidelines on analysis of extremes in a changing climate in support of informed decisions for adaptation. *World Meteorological Organization (WMO)*, WMO/TD-No. 1500: WCDMP-No. 72.